Check for updates

Received: 3 December 2021 | Revised: 24 January 2022 | Accepted: 29 March 2022

DOI: 10.1002/btpr.3253

RESEARCH ARTICLE

Cell Culture and Tissue Engineering

BIOTECHNOLOGY PROGRESS

A novel NCI-H69V small cell lung cancer functional mini-tumor model for future treatment screening applications

Liezaan van der Merwe[1] | Hanna Svitina[1,2] | Clarissa Willers[1] | Krzysztof Wrzesinski[1,3] | Chrisna Gouws[1]

[1]Centre of Excellence for Pharmaceutical Sciences (Pharmacen™), North-West University, Potchefstroom, South Africa

[2]Laboratory of Biosynthesis of Nucleic Acids, Department of Functional Genomics, Institute of Molecular Biology and Genetics of NASU, Kyiv, Ukraine

[3]CelVivo ApS, Blommenslyst, Denmark

Correspondence
Chrisna Gouws, Centre of Excellence for Pharmaceutical Sciences (Pharmacen™), North-West University, Private Bag X6001, Potchefstroom 2520, South Africa.
Email: chrisna.gouws@nwu.ac.za

Funding information
National Research Foundation (NRF) of South Africa, Grant/Award Numbers: 116353, 141964; South African Medical Research Council

Abstract

Small cell lung cancer (SCLC) is aggressive and despite multiple clinical trials, its standard of care is unchanged for the past three decades. In vitro cancer models are crucial in chemotherapy development, and three-dimensional (3D) models aim to bridge the gap between two-dimensional (2D) flat cultures and in vivo testing. Functional 3D spheroids can better represent the in vivo situation and tumor characteristics than 2D models. An NCI-H69V SCLC mini-tumor model was developed in a clinostat-based rotating bioreactor system. Spheroid growth and viability were characterized for 30 days, and the ideal experimental window with mature and metabolically stable spheroids was determined. Application of the model for anticancer treatment screening was validated with the standard chemotherapeutic drug irinotecan, for an exposure period of 72 h. The following parameters were measured: soluble protein content, planar surface area measurements, intracellular adenosine triphosphate and extracellular adenylate kinase levels, and glucose consumption. Histological morphology of the spheroids was observed. The established model proved viable and stable, while treatment with irinotecan caused a decrease in cell growth, viability, and glucose consumption demonstrating reactivity of the model to chemotherapy. Therefore, this NCI-H69V SCLC functional spheroid model could be used for future anticancer compound screening.

KEYWORDS
cancer model, functional spheroid, rotating bioreactors, small cell lung cancer, three-dimensional cell culture

1 | INTRODUCTION

Lung cancer is still one of the most aggressive malignancies in the world, with a high morbidity and mortality rate and 58% of cases occurring in less developed countries.[1–3] Lung cancer diagnoses are divided into small cell lung cancer (SCLC) and other forms of lung cancer, collectively known as non-small cell lung cancers (NSCLC).[4] SCLC makes up 15%–20% of all lung cancer cases and has one of the highest case-fatality rates, with deaths nearly as many as diagnoses.[5–9] This cancer is a well-defined, major histologic type of epithelial tumor that expresses neuroendocrine cell differentiation.[4,10,11] Clinical characteristics of SCLC include a rapid doubling time and disease progression with early

This is an open access article under the terms of the Creative Commons Attribution-NonCommercial-NoDerivs License, which permits use and distribution in any medium, provided the original work is properly cited, the use is non-commercial and no modifications or adaptations are made.
© 2022 The Authors. *Biotechnology Progress* published by Wiley Periodicals LLC on behalf of American Institute of Chemical Engineers.

dissemination to metastatic sites.[8–10,12] Although the 5-year survival rate of extensive stage-SCLC patients improved from 4.9% in 1983 to 6.4% in 2012, the median survival (time from diagnosis when half of the patients are still alive) remained <10 months. This was despite more than 52 randomized stage three clinical trials conducted in the past three decades.[4,5,13–15] The standard treatment for SCLC involves both chemotherapy and chest radiotherapy, with an initial good response of 70%–90% to this first-line treatment, but is followed by a recurrence of the disease within 2 years that is often more resistant to first-line therapy with a response rate of only 17%.[6,8,9,12,16,17] The first-line chemotherapy regimen for SCLC, since the 1980's, is a combination of cisplatin and etoposide that induces DNA damage leading to apoptosis.[5,9,18] Improvement of the long-term survival of patients depends on the development of new therapeutic regimens and approaches to overcome the challenge of resistance to chemotherapeutic drugs.[19]

Irinotecan is a water-soluble derivative of camptothecin that is hydrolyzed by the enzyme carboxylesterase (CE) to the highly active metabolite, 7-ethyl-10-hydroxycamptothecin (SN-38).[20–22] Irinotecan is used for the treatment of colorectal cancer and other solid tumors and is one of the most important drugs in the treatment of SCLC.[9,16,23] The most prevalent treatment-induced adverse effects of irinotecan are myelosuppression (predominantly leukopenia) and acute or chronic diarrhea, which has led to poor patient compliance.[16,21] The mechanism of action of irinotecan and its active metabolite entails the inhibition of DNA topoisomerase 1 (Topo 1) activity that causes cell cycle arrest and cell death.[21,23] Irinotecan was found to be more active in SCLC tumors compared to NSCLC malignancies, due to the higher levels of CE found in SCLC (specifically also in the NCI-H69 cell line), and consequently higher levels of intracellular conversion to the active metabolite.[15,20] CE activity in SCLC was found to be comparable to colorectal and pancreas tumor CE activity, wherein irinotecan showed clinical efficacy.[15] For second-line therapy, irinotecan treatment had similar results to that of topotecan, also a camptothecin derivative, and is therefore included in the standard treatment of recurrent SCLC.[5,15,24] Irinotecan caused more gastrointestinal side-effects in patients, while etoposide caused more hematological side-effects, therefore irinotecan is recommended as alternative treatment in the case of contraindications to etoposide.[25]

Clinical trials have proved to be a long and costly process with oftentimes disappointing results, especially considering the high attrition rates in cancer drug discovery.[26–29] Moreover, the United States Environmental Protection Agency announced 2035 as the deadline for the elimination of animal models in research, starting with the phase out of animal models from 2025 by limiting funding.[30] This places the urgent development of reliable and reproducible cell-based pre-clinical models in a new light. The development of in vitro cancer models, that accurately represent the tumor in question, can help to identify compounds that lack efficacy and safety during the pre-clinical stage ensuring further development of more promising therapies.[26,31] Tumor-derived cell lines have been used as the gold standard for cytotoxicity testing since the 1950's owing to their simplicity, versatility, and reproducibility.[32,33] However, three-dimensional (3D) cancer cell models have been found to better represent in vivo solid tumors than two-dimensional (2D) tumor-derived cell lines, as most tumors grow three-dimensionally and consist of complex interactions between cells and their environment.[31,34] The cell morphology, polarity, receptor expression, oncogene expression, and overall architecture of 3D systems are reflective of in vivo tumors.[26,35] Multiple SCLC cell lines have been established from tumors. The NCI-H69V cell line was established from the parent cell line, NCI-H69, and while the parent cell line grows as floating-cell aggregates, the NCI-H69V cells grow adherent to a substrate or surface.[36] Key differences evident in the NCI-H69V adherent cell line, compared to the parent cell line, is the low expression of the epithelial marker gene, E-cadherin, and the strong expression of vimentin and other epithelial-mesenchymal transition (EMT) inductors and effectors that indicate the transition from epithelial parent cells into a mesenchymal phenotype seen in NCI-H69V cells. The NCI-H69V cells also express low levels of neuroendocrine markers, compared to NCI-H69.[36,37] EMT is associated with a higher potential for the migration and invasion of tumor cells as well as the development of chemoresistance during treatment; this was observed in the NCI-H69V cell line, but not the NCI-H69 parent cell line.[36,38,39] The presence of this subpopulation of cells (NCI-H69V) in SCLC tumors can be the reason why a good initial response to chemotherapy is seen, followed by a relapse and poor prognosis.[36]

In this study, NCI-H69V cells were cultured as irrigated functional spheroids. Spheroids form through the aggregation of cells into a spherical geometry with a concentric arrangement of cell layers within the spheroid.[27] Usually this consists of a necrotic core, followed by a layer of senescent cells and then the layer of proliferating cells, but it depends on the method of culturing and the size of the spheroids.[40] This layering, together with the formation of nutrient and waste gradients due to diffusion limits in bigger spheroids, affects the distribution, activation and metabolism of drug compounds in spheroids heterogeneously.[41] Several methods exist for scaffold-free spheroid formation and can be divided into static and dynamic culture systems.[42] Dynamic culture methods include the spinner flask, rotating system, and microfluidic system.[27] In this study, a dynamic clinostat-based rotating bioreactor and BioArray Matrix (BAM) drive system were used for the formation and maintenance of NCI-H69V mini-tumors.[43–45] Bioreactors use a slow rotation of the vessel to create a simulated microgravity environment that keeps cells in suspension, while allowing aggregation into spheroids.[42] A controlled environment with the continuous flow of culture media, homogeneous distribution of dissolved compounds and gasses, efficient delivery of nutrients to cells and waste removal from cells are provided by bioreactors.[46,47] The objectives of this study were to characterize the growth and viability of a new functional NCI-H69V spheroid model, before validating its use as a cancer treatment screening tool by evaluating the reactivity of the spheroids when treated with the standard chemotherapeutic drug, irinotecan.

2 | MATERIALS AND METHODS

2.1 | Materials

Materials and reagents used included phosphate buffered saline (PBS) (Hyclone; Separations, Johannesburg, South Africa), Trypsin-Versene

15206033, 2022, 4, Downloaded from https://aiche.onlinelibrary.wiley.com/doi/10.1002/btpr.3253 by Royal Danish Library, Wiley Online Library on [23/04/2026]. See the Terms and Conditions (https://onlinelibrary.wiley.com/terms-and-conditions) on Wiley Online Library for rules of use; OA articles are governed by the applicable Creative Commons License

(EDTA) (Lonza; Whitehead Scientific [Pty] Ltd., Cape Town, South Africa), Triton™ X-100 (Merck, Sigma-Aldrich, Johannesburg, South Africa), 3-(4,5-dimethylthiazol-2-yl)-2,5-diphenyl tetrazolium bromide (MTT) powder (Merck, Sigma-Aldrich) and L-ascorbic acid (Merck, Sigma-Aldrich). Bioreactors were purchased from CelVivo® ApS (Odense, Denmark). The Quick Start™ Bradford Protein assay and 2 mg/ml bovine serum albumin (BSA) standard was purchased from Bio-Rad (Lasec SA [Pty] Ltd., Midrand, South Africa). The lysis buffer was donated by Celvivo® ApS (Odense, Denmark). The CellTiter-Glo® luminescent cell viability assay was supplied by Promega (Anatech Instruments [Pty] Ltd., Johannesburg, South Africa) and the ATP disodium salt hydrate standard was purchased from Merck, Sigma-Aldrich. The ToxiLight® BioAssay kit was purchased from Lonza (Whitehead Scientific [Pty] Ltd.).

2.2 | Two-dimensional culturing of NCI-H69V cells

The NCI-H69V cells (purchased from the European Collection of Authenticated Cell Cultures [ECACC], Cat# 91091803, Public Health England, UK), was cultured using standard culturing conditions. The culture medium, Roswell Park Memorial Institute (RPMI 1640) medium (Gibco, Thermo Fisher Scientific, Johannesburg, South Africa) was supplemented with 10% fetal bovine serum (FBS) (Gibco, Thermo Fisher Scientific), 1% non-essential amino acids (NEAA) (Lonza; Whitehead Scientific [Pty] Ltd.), 1% penicillin/streptomycin (10,000 U of each/ml, Lonza; Whitehead Scientific [Pty] Ltd.) and 2 mM L-glutamine (Lonza; Whitehead Scientific [Pty] Ltd.). Cultures were incubated in a Forma Steri-Cycle CO_2 Incubator (Thermo Fisher Scientific; Marietta) at 37°C with 5% CO_2 and 95% humidified air, with the culture medium exchanged every second day. Sub-culturing of the cells was initiated upon reaching 80%–90% confluence by trypsinization, using 0.25% Trypsin-Versene.

2.3 | Two-dimensional anticancer activity pre-screening

For the MTT assay, 6000 cells per well were seeded in 96-well plates and incubated at 37°C, 5% CO_2 and 95% humidified air for 24 h to allow adherence of the cells. Culture medium was replaced with 200 µl culture medium containing irinotecan hydrochloride (Merck, Sigma-Aldrich) at various concentrations (this was considered as 0 h). This treatment-containing medium was replaced in 24 h intervals until the assay was performed after a 96 h total exposure time. The following controls were included: untreated controls (to indicate 100% viability), dimethyl sulfoxide (DMSO) blank control wells (cells treated with DMSO to eliminate background interference) and dead cell control wells (cells treated with Triton™ X-100 to indicate 97%–100% relative cell viability inhibition).

Irinotecan hydrochloride stock solution was prepared in DMSO and stored at −20°C. Prior to each daily dosing, an aliquot of the stock solution was thawed at room temperature (22°C) and diluted to a concentration range of 1.5×10^{-7} M–9.5×10^{-7} M (150–950 nM) using culture medium.

After 96 h exposure, medium was removed from all the wells and the cells were washed twice with pre-warmed PBS. The dead cell control wells were treated with 200 µl of 0.2% Triton™ X-100 (dissolved in PBS) for 15 min, and subsequently carefully washed twice with PBS. Thereafter, 180 µl non-additive medium was added to all the wells. The MTT stock solution of 5 mg/ml was administered at a volume of 20 µl to each well (excluding the DMSO blank control wells) to achieve a final MTT concentration of 0.5 mg/ml.[45,48,49] The plate was covered and placed on a compact rocker for 5 min, followed by further incubation at 37°C for 4 h. After incubation, the content of each well was removed and 200 µl DMSO was added to each well to dissolve the formed crystals. The plate was shaken on a compact rocker for a further 1 h. The amount of formed formazan crystals that accumulated in each well, was quantified by measuring the absorbance at 560 nm, with a reference background wavelength of 630 nm using a SpectraMax® plate reader (Paradigm® Multi-Mode Detection Platform; Molecular Devices®; Separations, Gauteng, South Africa).

The measured absorbance values for each group were expressed as relative percentage viability of the cells, relative to the untreated control cells, using Equation (1),

$$\%\text{Cell viability} = \frac{(\Delta\text{sample} - \Delta\text{blank})}{(\Delta\text{untreated control} - \Delta\text{blank})} \times 100 \quad (1)$$

where Δ sample is the difference between the wavelength 560 nm value and that of the background wavelength (630 nm), measured for all the sample groups on the plate. Δ blank is the difference between the wavelength 560 nm value and that of the background wavelength of the DMSO control wells. Δ untreated control is the difference between the wavelength 560 nm value and that of the background wavelength measured for the untreated control group.

Thereafter, Equation (2) was used to determine the relative percentage cell viability inhibition (IC).

$$\%\text{IC} = 100\% - \%\text{cell viability} \quad (2)$$

All MTT experiments were performed twice, with three replicates for each experiment (six replicates for each concentration). SPSS statistical analysis software (IBM Analytics, Version 25), in conjunction with the Probit Analysis Method, were used to calculate IC_{25}, IC_{50}, and IC_{75} values with 95% confidence limit ranges for irinotecan hydrochloride, using the data from the MTT analyses.

The IC_{25} and IC_{50} values, recounted to µg irinotecan hydrochloride, were then divided by the measured soluble protein content (µg) of the 6000 cells seeded per well for the MTT experiments. This was done to obtain the µg drug per µg of soluble protein for the calculated IC_{25} and IC_{50} values of the treatment.

2.4 | Preparation of rotating bioreactors

Bioreactors were prepared 24 h before adding the cell suspension. The humidity chambers were filled with sterile distilled water. The cell

15206033, 2022, 4, Downloaded from https://aiche.onlinelibrary.wiley.com/doi/10.1002/btpr.3253 by Royal Danish Library, Wiley Online Library on [23/04/2026]. See the Terms and Conditions (https://onlinelibrary.wiley.com/terms-and-conditions) on Wiley Online Library for rules of use; OA articles are governed by the applicable Creative Commons License

chambers were rinsed with sterile distilled water and then filled with 5 ml non-additive culture medium. The bioreactors were placed onto the drive-unit of the BAM system (BAM v 4.6; CelVivo® ApS) in an ESCO Cell Culture CO_2 incubator (Changi, Singapore) to rotate and equilibrate overnight at a rotation speed of 15 rotations per minute (rpm) at 37°C, 5% CO_2 and 95% humidified air.[45,50,51]

2.5 | NCI-H69V spheroid formation and maintenance

An NCI-H69V single cell suspension was prepared by trypsinization and counted with a Scepter™ 2.0 handheld automated counter (Millipore, MA). A 1×10^5 cells/ml suspension was prepared and added to each prepared bioreactor with a total volume of 10 ml. Culture medium used for initiation of spheroids was supplemented with 25 μg/ml ascorbic acid. Ascorbic acid was added to the culture medium to assist in better ECM production resulting in more structurally sound spheroids, since it plays a role in in the folding and deposition of collagen proteins, which impacts the extracellular matrix (ECM).[52] Bioreactors were rotated at 2.5 rpm for 72 h. Following this incubation period, the formed spheroids were transferred to a 6-well plate containing pre-warmed culture medium. Spheroids were visually inspected for uniformity and perceived density using a Nikon Eclipse TS100 inverted light microscope (Nikon Instruments, Tokyo, Japan). Spheroids of similar sizes were then selected and counted, before being placed in prepared bioreactors with pre-warmed culture medium supplemented with 5 μg/ml ascorbic acid for maintenance. The bioreactors were returned to the drive units rotated initially at 8.0–8.5 rpm. Day 0 was defined as the day the formed spheroids were transferred to the newly prepared bioreactors. pH equilibrated culture medium, containing 5 μg/ml ascorbic acid, was exchanged every second day and the rotation speed adjusted daily to keep the spheroids suspended in the culture medium. Photomicrographs of the developing spheroids were taken using the Nikon Eclipse TS100 inverted light microscope and a DFK 72AUC02 USB 2.0 color industrial camera (The Imaging Source, Bremen, Germany).

2.6 | Characterization of the NCI-H69V spheroid model

The NCI-H69V spheroids had to be characterized to observe spheroid growth and cell viability, and to establish the optimal experimental window. The parameters measured were intracellular adenosine triphosphate (ATP), extracellular adenylate kinase (AK), soluble protein, glucose content of spent media,[51] as well as planimetric measurements of sampled spheroids. On day 0, 300 spheroids were transferred to each bioreactor, and two biological experimental replicates (each consisting of two bioreactors) were prepared for characterization. Sampling took place every second day, alternating between the two bioreactors from each experimental replicate, for a period of 30 days. After sampling on day 8, the content of each bioreactor was reduced to 130 spheroids per bioreactor to manage the spheroid density. Following splitting on day 8, there were subsequently three experimental replicates with each consisting of two bioreactors. On day 18, the spheroid population was reduced again to only 70 spheroids per bioreactor. It is important to note that once established as individual spheroids, each spheroid is considered an individual entity which develops and adapts independent from the other spheroids. That is why both biological repeats (replicate individual bioreactors per sample group) and technical repeats (number of spheroids/samples) are used.

Each assay consisted of three sampled groups (technical replicates) from each experimental replicate. Therefore, from day 0 to 8 there were six sampled groups in total, and from day 10 to 30 there were nine sampled groups in total. On day 0, sampling in triplicate from each experimental replicate consisted of two spheroids each, for the soluble protein and the intracellular ATP assay. From day 2 to 8 sampling in triplicate from each experimental replicate entailed one spheroid for the soluble protein assay and two spheroids for the intracellular ATP assay. From day 10 onwards, sampling in triplicate from each experimental replicate consisted of one spheroid each for the soluble protein and intracellular ATP assay. For the duration of the characterization, 200 μl spent medium was sampled from every experimental replicate for the extracellular AK assay and the remainder of the spent medium was used for glucose content and pH measurements. Glucose content of the spent media was measured in duplicate.

2.6.1 | The Bradford soluble protein assay

The Bradford protein assay was used to measure the amount of soluble protein in each spheroid.[51] Seeing that it is nearly impossible to count single cells in the spheroid construct in a non-invasive manner, the measured soluble protein content also served as a way of determining biomass. Spheroids were sampled into a clear 96-well plate and photomicrographs taken of the spheroids using the Nikon Eclipse TS100 inverted light microscope and a DFK 72AUC02 USB 2.0 color industrial camera for planimetric measurements. Spheroids were washed with PBS and then immersed in 150 μl PBS in each sample well. Lysis buffer (10 μl) was subsequently added and the spheroids in each well lysed thoroughly by pipetting. Protein samples had to be diluted 1:2 on day 4, 1:3 on day 6, 1:4 on day 8 and day 10, 1:5 on day 12, 1:6 on day 14 and 1:7 from day 16 to 30. PBS was then added to each well to a final volume of 160 μl, followed by addition of the protein assay dye reagent (40 μl) and vigorous mixing. The plate was centrifuged at 1218 ×g for 2 min to remove all air bubbles. The absorbance was measured with a Spectramax® Paradigm plate reader at 595 nm, and the measured absorbance values were quantified relative to a

15206033, 2022, 4, Downloaded from https://aiche.onlinelibrary.wiley.com/doi/10.1002/btpr.3253 by Royal Danish Library, Wiley Online Library on [23/04/2026]. See the Terms and Conditions (https://onlinelibrary.wiley.com/terms-and-conditions) on Wiley Online Library for rules of use; OA articles are governed by the applicable Creative Commons License

BSA standard to determine the soluble protein content (μg) per spheroid for each sampling day.

2.6.2 | Planimetry

The spheroid planar surface area was measured after images were taken at 4× magnification, and ImageJ software was used to measure the planar surface area (μm^2) of each spheroid sampled for the soluble protein and intracellular ATP assay.[53] A calibration image was used to set the scale for measurement and the "oval, elliptical" tool or the "freehand" tool was used to encircle the spheroid shadowed area to measure the planar surface area.

2.6.3 | Histological analysis

On days 14, 18, and 26, spheroids were sampled for histological analysis and fixated in 10% buffered formalin for 7 days. The spheroids were dehydrated using a series of increasing percentage ethanol solutions and thereafter paraffin-embedded. Sections of 5 μm thick were cut and adhered to Thermo Scientific™ SuperFrost Plus™ Adhesion slides. After deparaffinization and rehydration, slides were stained with hematoxylin–eosin (HE) and alcian blue to examine spheroid morphology.

2.6.4 | Intracellular adenosine triphosphate cell viability assay

The ATP assay was performed directly after sampling to ensure accurate viability measurements of the spheroids.[51] An ATP standard concentration series was prepared and plated in duplicate (2 × 100 μl) in black, clear bottom 96-well plates. Photomicrographs were taken of the sampled spheroids for planimetric measurements and all culture medium then removed. Following the addition of 100 μl PBS to each sampled spheroid, 100 μl of CellTiter-Glo® luminescent lysis buffer was added to all wells and mixed vigorously to lyse the spheroids. The plate was covered and incubated in the dark for 40 min. The plate was then centrifuged at 1218 ×g for 2 min to remove all air bubbles. Luminescence was measured with a Spectramax® Paradigm plate reader and all samples were quantified relative to the known ATP standard. Samples were normalized relative to the soluble protein content per spheroid for each sampling day.

2.6.5 | Extracellular adenylate kinase cell death assay

Collected spent culture medium from each experimental replicate was centrifuged at 140 ×g for 5 min, and 160 μl of the supernatant was then transferred to new microcentrifuge tubes. The transferred samples were centrifuged at 19,480 ×g for 15 min, and 140 μl of the supernatant transferred to new tubes. These samples were then flash frozen with liquid nitrogen and stored at −80°C until the assay was performed.

All samples were equilibrated to room temperature (22°C), and each experimental replicate was plated in triplicate (20 μl per well) in black, clear bottom 96-well plates. A known dead cell standard was prepared by treating a known concentration of NCI-H69V cells with Cyto-Tox Glo® digitonin lysis buffer (Promega). The cell concentration in RPMI 1640 medium that was used was 3.78×10^5 cells/ml. The dead cell standard was then diluted with heat-treated medium and exposed to the same conditions as the samples. AK detection reagent (100 μl) was added to all wells and mixed. The plate was covered and placed on a compact rocker for 20 min, followed by centrifugation at 1218 ×g for 2 min to remove air bubbles. Luminescence was measured with a Spectramax® Paradigm plate reader and all samples were quantified relative to the known dead cell standard to determine the number of dead cells per ml of culture medium. This was multiplied by 10 in order to get the number of dead cells in total for each experimental replicate of 10 ml, which was then normalized to the total soluble protein content of each experimental replicate for each sampling day.

2.6.6 | Approximate glucose consumption

The OneTouch® Select™ blood glucose monitoring system and OneTouch® Select™ test strips were used to measure the glucose content of spent medium from each experimental replicate. This indicated the clearance of glucose from the medium.[51] Spent medium (3 μl) was loaded on the test strips and the glucose concentrations (mmol/L) noted. The glucose concentration of fresh culture medium was also measured and by deducting the remaining glucose content from this value, an approximation of the glucose consumption by the spheroids in each experimental replicate could be estimated. This was divided by the total soluble protein content of each experimental replicate to get an approximation of the glucose consumption per protein (μg).

2.7 | Validation of the NCI-H69V spheroid model for anticancer treatment screening

Validation of the NCI-H69V spheroid model for anticancer screening was done with the standard chemotherapeutic drug, irinotecan hydrochloride. The setup and maintenance of the bioreactors were the same as for characterization. During this experiment, each of the treatment groups consisted of two bioreactors (biological replicates). On day 14 of spheroid culture, all the spheroids were removed from the bioreactors and pooled together in fresh, pre-warmed culture medium. Subsequently, 90 spheroids were placed in each bioreactor, which was then filled with pre-warmed culture medium and returned to the drive unit where the speed was

15206033, 2022, 4, Downloaded from https://aiche.onlinelibrary.wiley.com/doi/10.1002/btpr.3253 by Royal Danish Library, Wiley Online Library on [23/04/2026]. See the Terms and Conditions (https://onlinelibrary.wiley.com/terms-and-conditions) on Wiley Online Library for rules of use; OA articles are governed by the applicable Creative Commons License

adjusted until day 16. Treatment with irinotecan hydrochloride started on day 16 (seen as 0 h) and sampling took place following 0, 24, 48, and 72 h of exposure. All experimental procedures were the same as described for characterization.

2.7.1 | Treatment dose calculations

The daily measured soluble protein content was used to determine the total biomass in each bioreactor, and the treatment was then adjusted to dose per protein (μg) for each bioreactor. The soluble protein content (μg) per spheroid was multiplied by the number of spheroids in each bioreactor per day, to obtain the total protein (μg) per bioreactor, and the dose of irinotecan hydrochloride was adapted accordingly. This ensured that the spheroids were constantly exposed to a consistent amount of irinotecan for the duration of the experiment.

After sampling for the soluble protein, intracellular ATP, and extracellular AK assays, the bioreactors were filled with the prepared treatments of the previous day. Once the soluble protein content for each bioreactor was determined and the new dose per bioreactor calculated, the medium of each bioreactor was exchanged with the new treatment-containing culture medium. The treatment dosages were based on the IC_{25} and IC_{50} concentrations for irinotecan, as determined with the MTT assay. The treatment groups and their dosages per protein were categorized as an untreated control, irinotecan hydrochloride $[IC_{25}] = 8.89 \times 10^{-3}$ μg irinotecan hydrochloride/μg protein, and irinotecan hydrochloride $[IC_{50}] = 2.06 \times 10^{-2}$ μg irinotecan hydrochloride/μg protein.

2.7.2 | Statistical data analysis

Data analysis was performed with Statistica v.13.3 software (TIBCO Software Inc., 2018, http://statistica.io.). The technical replicates values from two or three different bioreactors were combined, therefore, a minimum of six spheroids ($n = 6$) were analyzed in each assay. One-way ANOVA, followed by the Dunnett post hoc test for comparison of multiple groups with a control group (day 0 for all, except for glucose consumption where it was compared to day 2) was used for analysis of the characterization data. One-way ANOVA followed by the Tukey post hoc test for comparison of multiple groups was used for analysis of the spheroid model validation data. Differences were considered statistically significant when $p < 0.05$.

3 | RESULTS

A novel 3D NCI-H69V SCLC mini-tumor model was established and characterized in terms of growth and viability by measuring the intracellular ATP content, extracellular AK release, glucose consumption, soluble protein content, and planar surface area of the spheroids. To validate the model for use in anticancer treatment efficacy screening, the standard chemotherapeutic drug, irinotecan hydrochloride, was used as a model drug in order to establish the reactivity of the spheroids towards treatment.

TABLE 1 The inhibitory concentrations of irinotecan hydrochloride, relative to an untreated control, in NCI-H69V cells as determined with Probit analysis

	Concentration (nM)	95% confidence limits (nM)
IC_{25}	248.2	178.1–306.1
IC_{50}	573.97	506.8–643.7

3.1 | Two-dimensional anticancer activity prescreening

The MTT assay was employed as a quick and easy screening tool to provide a general indication of the anticancer activity of irinotecan hydrochloride in 2D cultures of the NCI-H69V cell line. The cells were treated with increasing concentrations of irinotecan hydrochloride for 96 h, and the viability of the cells assessed after the exposure time. The data, expressed as a relative percentage viability inhibition at corresponding doses, were analyzed with the Probit regression analysis tool to calculate the 25% and 50% inhibitory concentration (IC_{25} and IC_{50}, respectively) per protein content for the NCI-H69V cell line, relative to an untreated control, with 95% confidence limits (given in Table 1).[54]

3.2 | Characterization of the NCI-H69V spheroid model

The NCI-H69V spheroids were formed from a single cell suspension in culture media containing 25 μg/ml ascorbic acid, and left to rotate in the bioreactors at a low rotation speed for 72 h. A high yield of dense spheroids was produced, sorted according to size (Figure 1a) and further maintained in bioreactors. The growth and viability of the spheroids were assessed to clarify how the spheroids mature, when the spheroid density in the bioreactors should be decreased and when the spheroids were not viable anymore. On day 8, the spheroid population was reduced in each bioreactor to increase the availability of nutrients to the cells. Because size variation could still be observed in the first week of spheroid maintenance (Figure 1b), spheroids of similar size were chosen on day 8 for further maintenance. The spheroid population was decreased again on day 18 and size variation was less visible at this point (Figure 1c). From day 22 onwards, in addition to the mature spheroids (Figure 1d), the formation of "daughter" spheroids could be observed in all bioreactors (Figure 1f). Upon removal of the spent media from each bioreactor on day 24 to day 30, it was centrifuged and the cell pellet resuspended to evaluate the viability of the non-spheroid cells via trypan blue staining. Approximately 66% of the cells found in the media were cells with compromised cell membranes. The spheroid cultures were terminated on day 30.

3.2.1 | Soluble protein content

On day 0, 300 spheroids were placed in each bioreactor and the soluble protein content measured every second day. The protein content per spheroid increased consistently until day 6, followed by a decrease in

15206033, 2022, 4, Downloaded from https://aiche.onlinelibrary.wiley.com/doi/10.1002/btpr.3253 by Royal Danish Library, Wiley Online Library on [23/04/2026]. See the Terms and Conditions (https://onlinelibrary.wiley.com/terms-and-conditions) on Wiley Online Library for rules of use; OA articles are governed by the applicable Creative Commons License

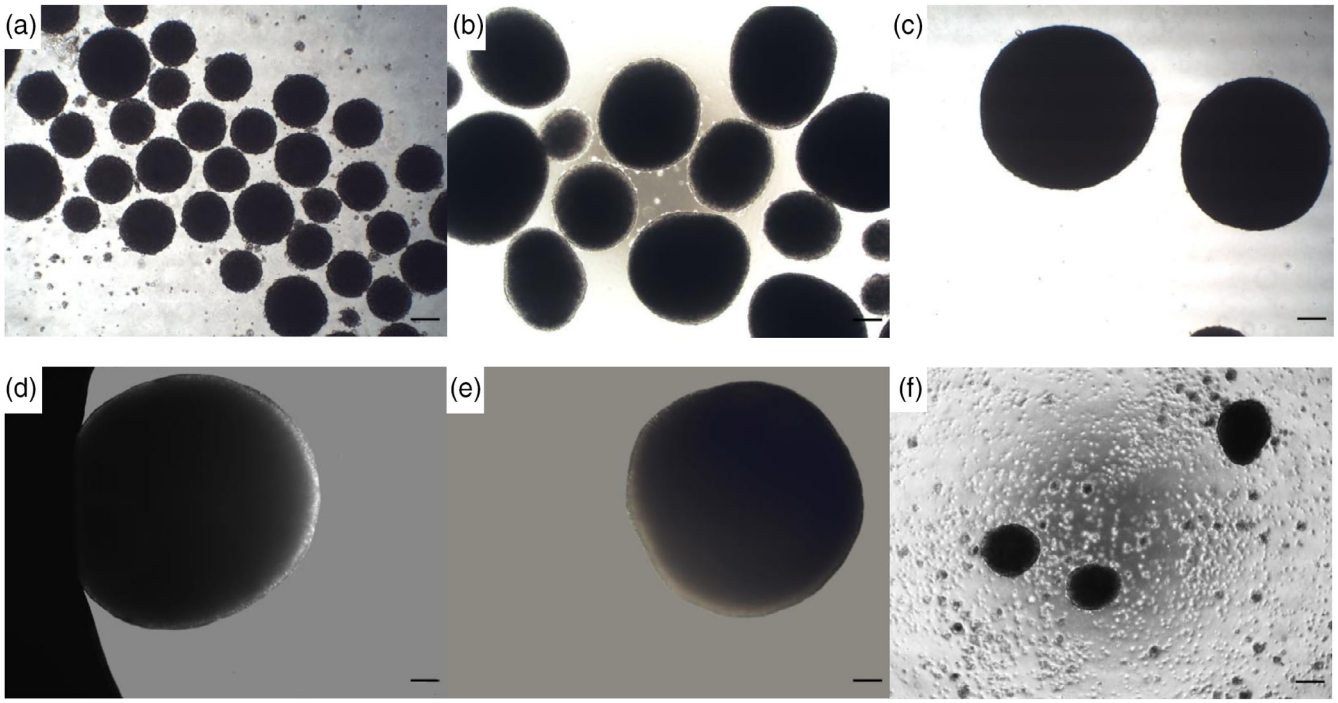


FIGURE 1 Photomicrographs of NCI-H69V spheroids during characterization, taken on (a) day 0, (b) day 8, (c) day 18, (d) day 22, and (e) day 30. (f) Shows the formation of "daughter" spheroids from day 22 until day 30 of culture in the rotating bioreactors (scale bar = 200 μm)

protein content on day 8 (Figure 2a). After sampling on day 8, the population of spheroids in each bioreactor was reduced to 130 spheroids. This led to a substantial increase in soluble protein content per spheroid from days 10 to 14, probably due to a greater availability of nutrients per cell. This was followed by some stabilization in protein content per spheroid from days 14 to 18. After sampling on day 18, the spheroid population was reduced to only 70 spheroids per bioreactor. This resulted in the second, although less pronounced, increase in soluble protein content from day 20 to day 26. From day 28, a reduction in protein content per spheroid was observed.

3.2.2 | Planimetry

The planar surface area (μm^2) was measured of each spheroid, sampled for the protein and ATP assays and was used as a tool to determine the size of the growing spheroids. A steady increase in surface area was seen from days 0 to 6, with the surface area then staying constant until day 8 (Figure 2b). After reducing the spheroid population in the bioreactors on day 8, there was a steady increase in the size/surface area of the spheroids again until day 22. The spheroid size seemed to even out from day 22 to 24, before increasing again from day 26 onward. Overall, the surface area of the spheroids increased almost linearly ($R^2 = 0.9854$) over the characterization period of 30 days.

3.2.3 | Histology

NCI-H69V spheroids were sampled on days 14, 18, and 26 for histological staining with HE to observe the morphology and organization of cells in the spheroids. Alcian blue staining was performed to identify the presence of mucin. On day 14, a definite lining of cells forming the outer rim of the spheroids could be seen, followed by a layer of proliferating cells and no obvious necrosis in the core (Figure 3a,d). There was also no mucin present in the spheroids (Figure 3a). The spheroids on day 18 presented with areas of what seems to be stroma in the periphery of the spheroid, with a definite border of cells forming the outer rim (Figure 3b,e). The presence of mucin, interwoven between the cells and concentrated in the center of the spheroids and in the area with "stroma" was indicated by the faint blue staining in Figure 3b. On day 26, the spheroids started to lose their shape. The outer rim of cells appeared to "break" at certain points and the "stroma" filled areas were bigger. The density of cells in the spheroids also appeared to be less than what was seen on days 14 and 18 (Figure 3c,f). Mucin was clearly present as indicated by the darker blue staining (Figure 3c), concentrated in the center of the spheroids, with the periphery still containing a relatively thick layer of proliferating cells. More necrotic areas could also be seen. The cells in all the spheroids appeared round, oval, or spindle-shaped with absent or inconspicuous nuclei, with what looks like nuclear molding as well as ill-defined cell borders.

3.2.4 | Intracellular adenosine triphosphate content

From day 2 to day 4 there was a marked increase in ATP content per protein as the spheroids adapted to the bioreactor environment and recovered from handling on day 0 (Figure 2c). On day 6 there was a decrease in ATP per protein, followed by a slight increase on day 8. After reducing the spheroid population on day 8, the ATP per protein content increased until day 14. After this, the ATP levels of the

15206033, 2022, 4, Downloaded from https://aiche.onlinelibrary.wiley.com/doi/10.1002/btpr.3253 by Royal Danish Library, Wiley Online Library on [23/04/2026]. See the Terms and Conditions (https://onlinelibrary.wiley.com/terms-and-conditions) on Wiley Online Library for rules of use; OA articles are governed by the applicable Creative Commons License

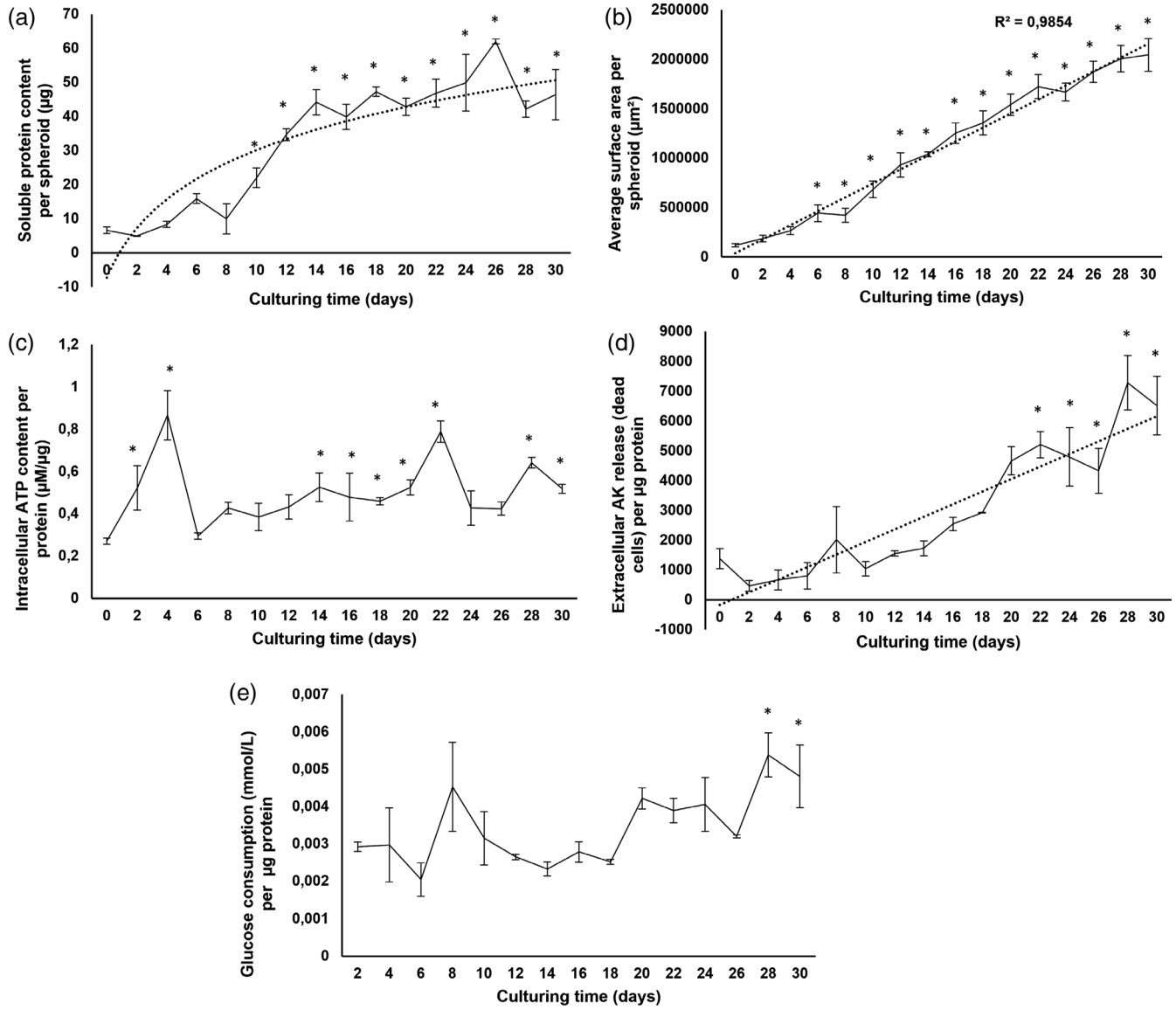


FIGURE 2 Characterization of the NCI-H69V spheroid model as a function of time, in terms of (a) soluble protein content per spheroid (µg); (b) measured planar surface area per spheroid (μm^2); (c) intracellular adenosine triphosphate content per soluble protein (µM/µg); (d) extracellular adenylate kinase release per µg protein; and (e) approximate glucose consumption (mmol/L) per µg protein ($n = 6$ for days 0–8 and $n = 9$ for days 10–30, error bars = *SD*; * = statistically significant, $p < 0.05$ [one-way ANOVA followed by the Dunnett post hoc test for comparison with day 0 for all, except glucose consumption compared to day 2])

spheroids stabilized until day 20. The second peak in ATP observed on day 22 could have been a result of the second reduction in the spheroid population on day 18.

3.2.5 | Extracellular adenylate kinase content

The AK release (representative of dead cells) per protein decreased from day 0 to day 2 and thereafter increased until a slight peak on day 8 (Figure 2d). After the spheroid population was reduced on day 8 there was again a slight decrease in AK per protein on day 10, followed by a steady increase until day 18. The second population reduction on day 18 resulted in an increase in AK per protein from day 18 to 22, possibly due to excessive handling of the spheroids. This was followed by a decrease in AK per protein until day 26 and then a sharp peak on day 28. Overall, the AK per protein content increased almost linearly over the characterization period of 30 days.

3.2.6 | Approximate glucose consumption

Quantification of glucose disappearance from the culture medium can be used as an indicator of metabolic activity, achieved by the estimation of glucose consumption during spheroid growth. The glucose content of

15206033, 2022, 4, Downloaded from https://aiche.onlinelibrary.wiley.com/doi/10.1002/btpr.3253 by Royal Danish Library, Wiley Online Library on [23/04/2026]. See the Terms and Conditions (https://onlinelibrary.wiley.com/terms-and-conditions) on Wiley Online Library for rules of use; OA articles are governed by the applicable Creative Commons License

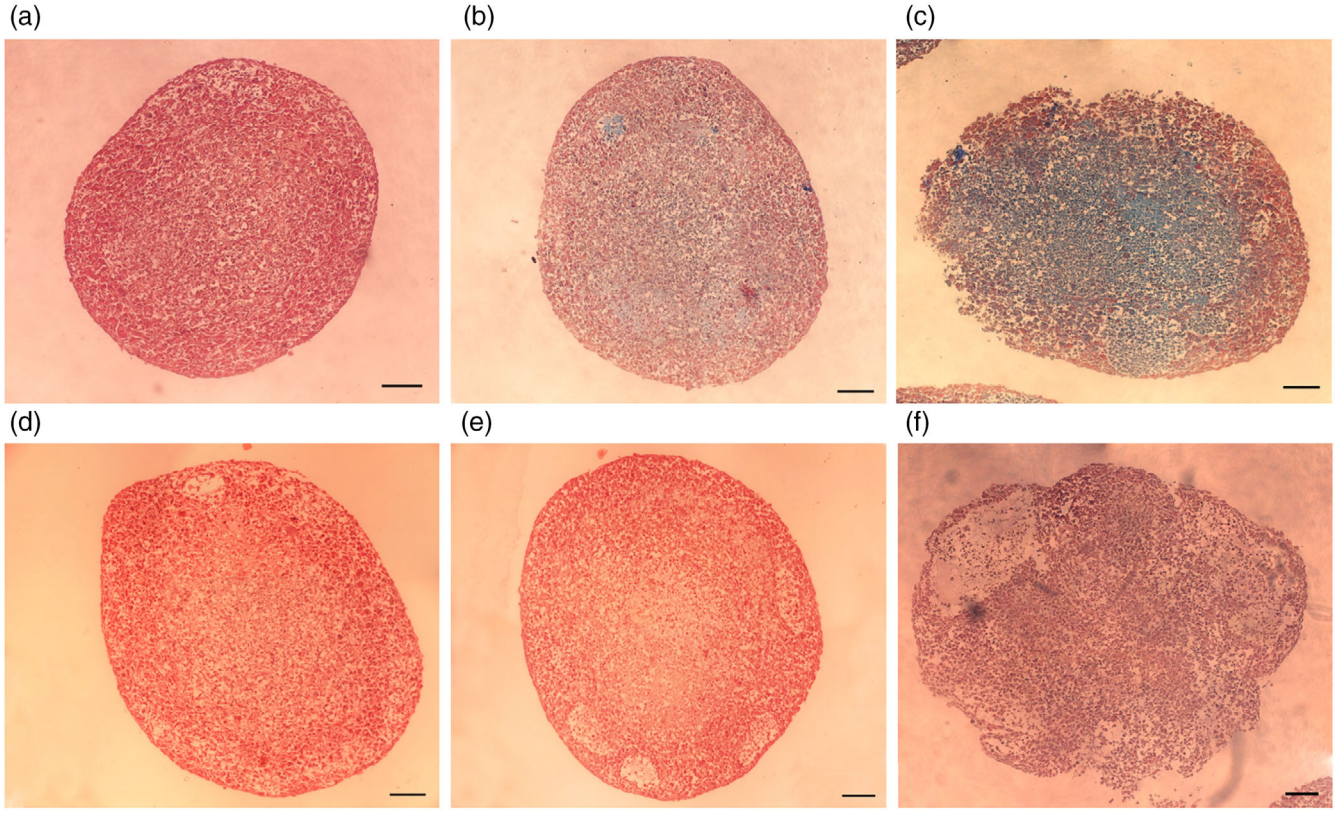


FIGURE 3 Histological staining of NCI-H69V spheroids with hematoxylin–eosin (HE) and alcian blue on (a) day 14, (b) day 18, and (c) day 26. NCI-H69V spheroids were stained with HE only, on (d) day 14, (e) day 18, and (f) day 26 (scale bar = 100 μm)

fresh culture medium supplied to the spheroids every second day was 13.7 mmol/L on average ($n = 5$). The glucose content in the spent media of each bioreactor was subtracted from this, in order to estimate the total consumption of glucose by the cells in the bioreactor. Glucose consumption was normalized relative to the total protein content in each bioreactor (number of spheroids × protein content per spheroid) to establish the estimated glucose consumption per protein (Figure 2e). In the first 4 days of culture in the bioreactors, glucose consumption appeared stable, followed by a slight decrease on day 6 and then a sharp peak on day 8. The reduction in spheroid population on day 8, resulted in a steadier glucose consumption from days 10 until 18. Further reduction of the spheroid population on day 18 resulted in an increase in glucose consumption per protein from day 20 to 24, with a significant increase in glucose consumption from day 28 to day 30, compared to day 2 ($p < 0.05$). From day 16 to day 30, the glucose content in the spent media was below detection limits, meaning almost all the glucose from the media has been consumed by the cells (data not shown).

3.3 | Validation of the NCI-H69V spheroid model for anticancer treatment screening

To validate the use of the model for future anticancer treatment efficacy screening, the standard chemotherapeutic drug, irinotecan hydrochloride, was used as a model drug. The reactivity of the NCI-H69V spheroid model to 72 h treatment with two different concentrations of irinotecan (IC_{25} and IC_{50}, based on 2D pre-screening data) was investigated to this end. All data was normalized to the untreated control group. The spheroid initiation and maintenance used for characterization was repeated for the validation experiment, and preparation of the treatment groups was done on day 14 of culture. Treatment was initiated on day 16 of culture (0 h). For the model to be useful in future anticancer research, it was expected that standard chemotherapeutic drugs used to treat SCLC should have a negative effect on the viability and proliferation of the NCI-H69V spheroids. Sampled spheroids were observed at each time point (every 24 h), and the damage caused by irinotecan hydrochloride on the NCI-H69V spheroids was clearly observed (as shown in Figure 4a). While the untreated control spheroids continued to grow after 48 and 72 h, the spheroids exposed to the two concentrations of irinotecan had compromised spheroid structure and a noticeable increase in debris and single cells in the bioreactors (Figure 4a).

3.3.1 | Planimetry

The planar surface area of all sampled spheroids was measured and the average surface area per spheroid for each group is displayed in Figure 4b. As expected, the control group spheroids showed an increase in surface area at each time point. The spheroid group

15206033, 2022, 4, Downloaded from https://aiche.onlinelibrary.wiley.com/doi/10.1002/btpr.3253 by Royal Danish Library, Wiley Online Library on [23/04/2026]. See the Terms and Conditions (https://onlinelibrary.wiley.com/terms-and-conditions) on Wiley Online Library for rules of use; OA articles are governed by the applicable Creative Commons License

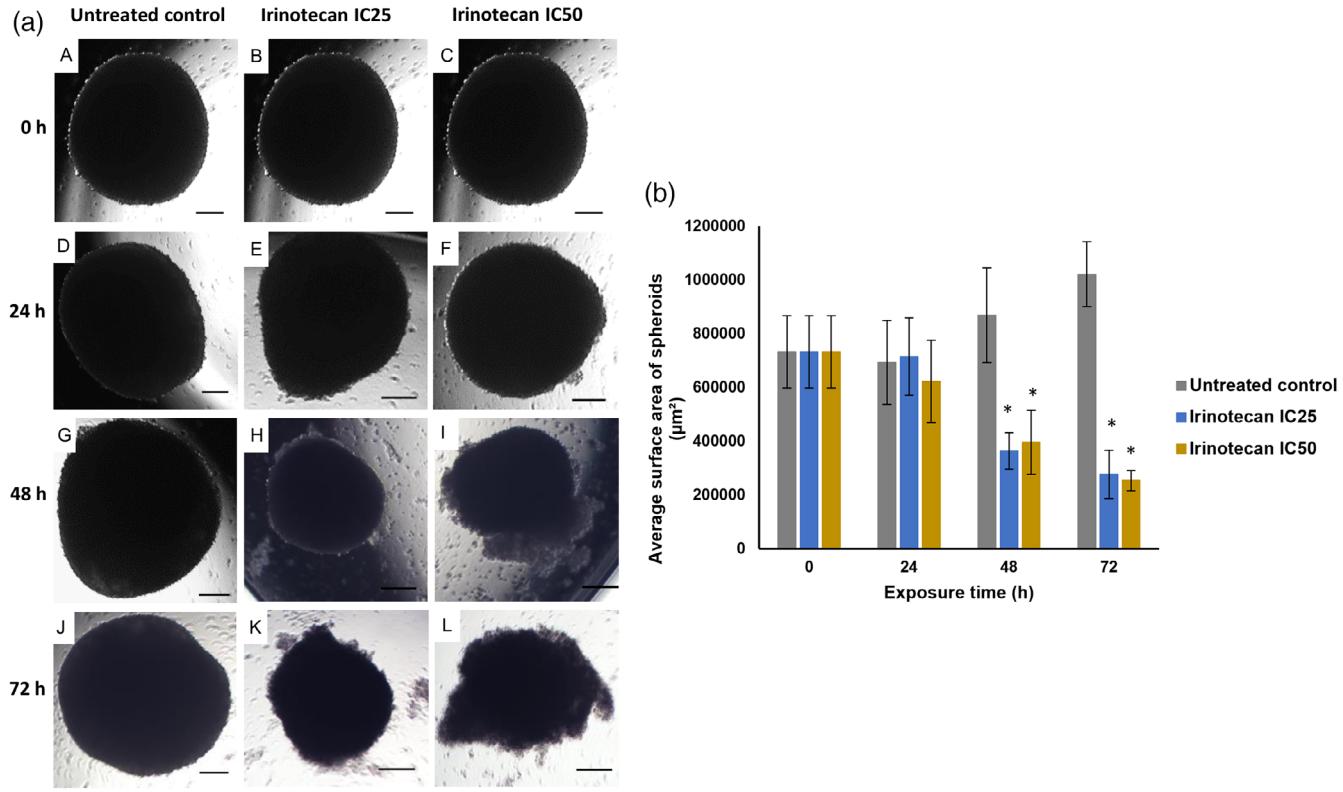


FIGURE 4 (i) Photomicrographs of spheroids during 72 h treatment (time 0 – a, b, c; 24 h – d, e, f; 48 h – g, h, i; 72 h – j, k, l) with irinotecan hydrochloride for the following treatment groups: untreated control (a, d, g, j) irinotecan IC_{25} (b, e, h, k) and irinotecan IC_{50} (c, f, i, l) (scale bar = 200 µm). (a), (ii) The average surface area per spheroid from each treatment group at each time point is shown (error bars = *SD*; $n = 6$; * = statistically significant, $p < 0.05$ [one-way ANOVA followed by the Tukey post hoc test for comparison with the untreated control at each time point])

exposed to irinotecan [IC_{25}] had the same surface area after 24 h exposure, but then there was a significant decrease in surface area after 48 h exposure with a further decrease after 72 h exposure ($p < 0.05$). The spheroid group exposed to irinotecan [IC_{50}] showed a decrease in surface area already after 24 h exposure, with a significant reduction after 48 h exposure followed by a further decrease after 72 h exposure ($p < 0.05$). After 72 h exposure, both treatment group spheroids had a comparable average surface area.

3.3.2 | Soluble protein content

Following exposure of the spheroids to irinotecan [IC_{25}] and irinotecan [IC_{50}], the soluble protein content was measured with the Bradford protein assay and the data normalized relative to the untreated control group. After 24 h exposure, the protein content of both treatment groups was already reduced relative to the control group, with the group exposed to irinotecan [IC_{25}] having a slightly higher protein content than the group exposed to irinotecan [IC_{50}] (Figure 5a). The soluble protein content decreased significantly after 48 h exposure to both treatment concentrations ($p < 0.05$). The group exposed to irinotecan [IC_{25}] had a lower protein content than those exposed to irinotecan [IC_{50}]. The protein content of the spheroid group exposed to irinotecan [IC_{25}] remained relatively unchanged after 72 h exposure, but the group exposed to irinotecan [IC_{50}] showed a further decrease in soluble protein content. The protein content after 48 and 72 h exposure to the treatment, for both treatment groups, were significantly reduced relative to the untreated control group ($p < 0.05$). It should be noted that the higher concentration treatment (IC_{50}) did not decrease the soluble protein content of the spheroids significantly more, than the lower concentration of the treatment (IC_{25}).

3.3.3 | Intracellular adenosine triphosphate content

After 24 h exposure, the ATP per protein content of the group exposed to the irinotecan [IC_{25}] decreased slightly more than the irinotecan [IC_{50}] group, although both decreased relative to the untreated control group (Figure 5b). The ATP per protein content of the irinotecan [IC_{50}] group stayed relatively constant for the remainder of the treatment. The group exposed to irinotecan [IC_{25}], however, had an increase in ATP per protein to more than the untreated control group after 48 h exposure. This was followed by a sharp decline after 72 h exposure to less than half the ATP per protein of the control group. None of these changes, however, were statistically significant compared to the untreated control group at each time point.

15206033, 2022, 4, Downloaded from https://aiche.onlinelibrary.wiley.com/doi/10.1002/btpr.3253 by Royal Danish Library, Wiley Online Library on [23/04/2026]. See the Terms and Conditions (https://onlinelibrary.wiley.com/terms-and-conditions) on Wiley Online Library for rules of use; OA articles are governed by the applicable Creative Commons License

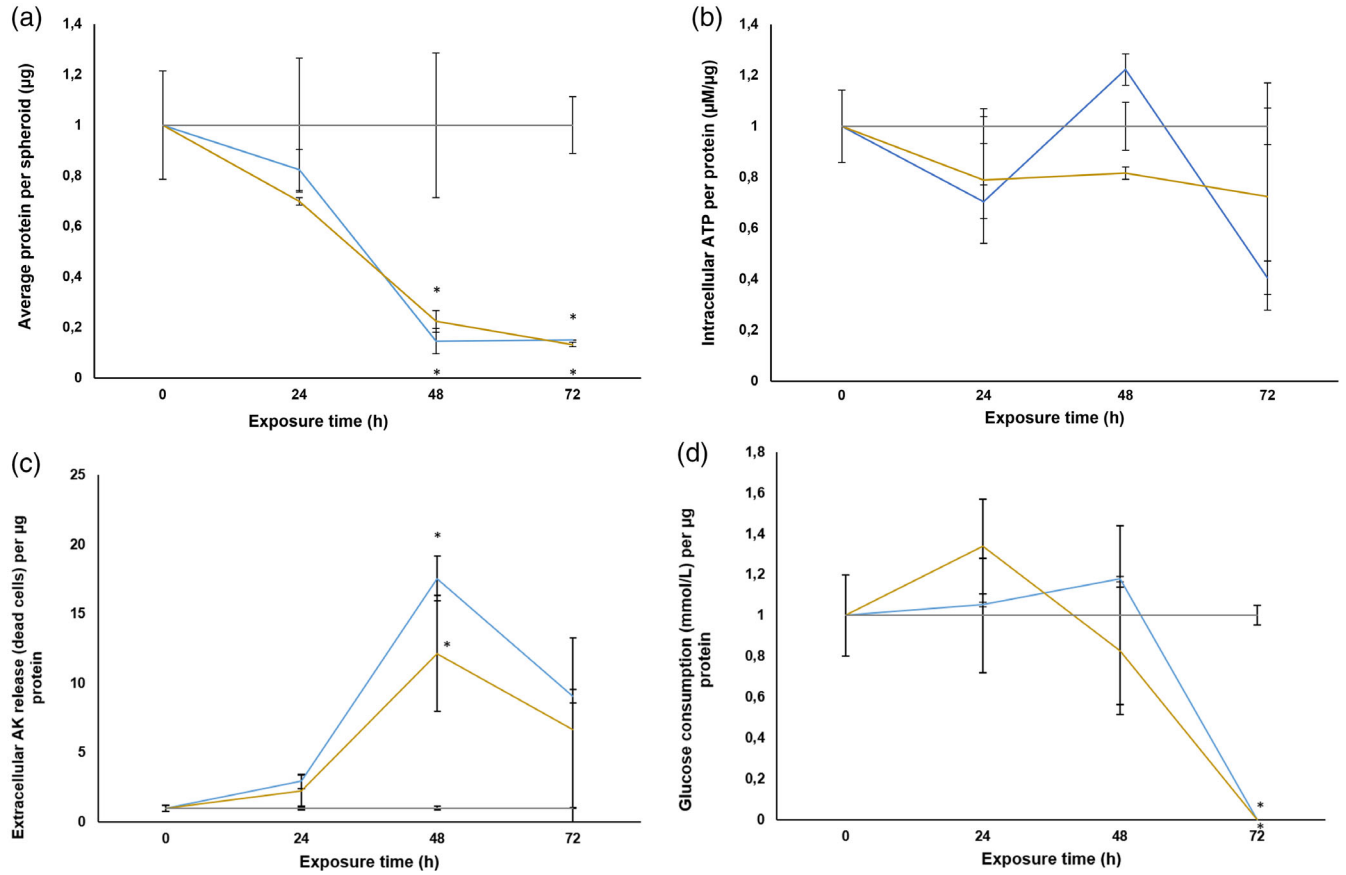


FIGURE 5 Validation of the NCI-H69V spheroid model with daily irinotecan treatments for 72 h, in terms of (a) normalized soluble protein content (µg) per spheroid; (b) normalized intracellular adenosine triphosphate content per soluble protein (µM/µg); (c) normalized extracellular adenylate kinase release per µg protein; and (d) normalized glucose consumption per µg protein. The untreated control group is shown in gray, the irinotecan [IC_{25}] group in blue and irinotecan [IC_{50}] group in yellow. All data was normalized relative to the untreated control group ($n = 6$, error bars = *SD*; * = statistically significant, $p < 0.05$ [one-way ANOVA followed by the Tukey post hoc test for comparison with the untreated control])

3.3.4 | Extracellular adenylate kinase content

The extracellular AK release for each treatment group was measured at each time point and expressed as AK per protein (µg), normalized relative to the untreated control group. After 24 h exposure to both concentrations of irinotecan, the treatment groups showed a slight increase in AK release compared to the untreated control (Figure 5c). After 48 h exposure there was a significant peak in AK release for both treatment groups ($p < 0.05$), with the irinotecan [IC_{25}] group having a higher peak than the irinotecan [IC_{50}] group. At the end of the treatment period, the AK release for both treatment groups decreased, but was still higher than the untreated control.

3.3.5 | Glucose consumption

The approximate glucose consumption of the spheroids in each treatment group (mmol/L) was expressed as glucose consumption per µg protein. The data were normalized relative to the glucose consumption per µg protein of the untreated control group. The spheroids exposed to irinotecan [IC_{25}] consumed slightly more glucose after 24 and 48 h exposure compared to the untreated control group (Figure 5d). The spheroids exposed to irinotecan [IC_{50}] consumed more glucose than both the irinotecan [IC_{25}] and control groups after 24 h exposure. However, after 48 h exposure, this group consumed less glucose than the other groups. Neither of the irinotecan treated groups consumed any glucose after 72 h exposure ($p < 0.05$).

4 | DISCUSSION

4.1 | Two-dimensional anticancer activity prescreening

Irinotecan hydrochloride cytotoxicity on a non-cancerous porcine embryonic kidney (LLC-PK1) cell line was previously investigated and the IC_{50} concentration was established as 15,534 nM, compared to the NCI-H69V cell line with an IC_{50} concentration of only 467 nM.[55] This provided insight on the selectivity of irinotecan towards these cancerous cells, as toxicity in the normal cells were observed only at much higher concentrations. The IC_{50} concentration determined in this study (573.97 nM – seen in Table 1) was comparable to that of

15206033, 2022, 4, Downloaded from https://aiche.onlinelibrary.wiley.com/doi/10.1002/btpr.3253 by Royal Danish Library, Wiley Online Library on [23/04/2026]. See the Terms and Conditions (https://onlinelibrary.wiley.com/terms-and-conditions) on Wiley Online Library for rules of use; OA articles are governed by the applicable Creative Commons License

Rossouw,[55] and falls within the range of 350–1500 nM for irinotecan IC_{50} concentrations determined in various SCLC cell lines.[20] The IC_{50} concentration was converted to an LD_{50} concentration of 2.06×10^{-2} μg irinotecan per μg protein (2.06×10^{-5} mg/mg protein) to facilitate comparison with dosages used in in vivo models and clinical studies, and to determine the dosages needed to treat the NCI-H69V spheroids. Dosages used in clinical trials are usually expressed as either mg per body surface area (mg/m^2) or as mg per body weight (mg/kg). Recommended clinical dosages of irinotecan as a single agent and in combination with carboplatin, is 100 and 50 mg/m^2, respectively.[56–58] Assuming the average height of a patient is 1.75 m and average weight is 75 kg, these dosages would be 2.54 mg/kg (2.54×10^{-3} mg/mg) and 1.27 mg/kg (1.27×10^{-3} mg/mg), respectively. In comparison to the dose determined in 2D NCI-H69V cells, the dose for irinotecan as a single agent used in clinical trials is about 100 times higher.

4.2 | Characterization of the NCI-H69V spheroid model

The NCI-H69V model was maintained and characterized for 30 days to evaluate the growth and viability of the spheroids. The significant increase in protein content per spheroid from day 10 correlate with the reduction in spheroid population on day 8, which in essence provided more space and nutrients for the cells to proliferate. The protein content per spheroid stabilized thereafter, an indication that the spheroids adapted to their environment in the bioreactor and the doubling time of the cells most probably decreased.[47] The presence of debris and single cells as well as the formation of daughter spheroids from day 22, however, complicates the determination of the total protein or total biomass in each bioreactor and results in greater variations in spheroid protein content. The planar surface area gives an indication of the size of the spheroids and is used as a tool to relate the protein content of spheroids to the size and to establish the correlation between these parameters.[50] The planar surface area of the NCI-H69V spheroids continued to increase linearly, while the protein content started to stabilize and plateau already at day 14. This could be a result of a decrease in spheroid density or compactness as the spheroids matured, as observed in Figure 3f where the 26-day-old spheroids lost their compact shape, and the density visibly declined. Histologically and cytologically, SCLC is characterized by scant cytoplasm, small nuclei with diffusely distributed and finely stippled chromatin, and absent or inconspicuous nucleoli.[10] The cells are small, round, ovoid, and spindle-shaped, and the in vivo tumors reach sizes of between 0.5 and 9 cm. The presence of single cell apoptosis or necrosis and intracytoplasmic mucin in the SCLC cells are also not uncommon.[59] Histological staining of the NCI-H69V spheroids (Figure 3) showed similarity to the typical characteristics of SCLC tumors, even the presence of mucin in the older spheroids, illustrating the capacity of 3D spheroids to mimic their tissue of origin.

Intracellular ATP content is a widely accepted method to indirectly determine the number of viable cells in both 2D and 3D cultures.[60,61] When the membrane integrity of cells is compromised, the cell loses the ability to produce ATP, and ATPases deplete remaining ATP in the cytoplasm.[48,62] AK is the enzyme that catalyzes the reaction necessary for ATP transfer from the mitochondria to local cellular processes, and also plays a role in regulating metabolic equilibrium within cells.[44,63] When cell membrane integrity is lost through direct damage or following cell death, AK will be released into the culture medium and can, therefore, serve as a parameter for cell death.[64] Due to the intertwined functions of these two parameters of cell viability, the interplay between both cell growth and cell death need to be considered when assessing cell viability. During characterization, the measured ATP and AK were normalized per μg protein to account for the growth of the spheroids. In the first 8 days, the spheroids were adapting to the environment in the bioreactor with ATP per protein peaking early on day 4, and AK increasing slowly until day 8. The maturation point for the NCI-H69V spheroids were from day 14 onward, as this was the point when ATP per protein and the protein content of the spheroids started to stabilize. The AK per protein increased steadily from day 14, but it was not significantly higher than day 0. Glucose consumption per protein also varied considerably until day 8, and stabilized from day 10. The active glucose consumption of the cells in the spheroid, together with the presence of ATP inside the cells indicated that the spheroids were viable and metabolically active, even though the AK content in the extracellular media increased slightly.

The formation of daughter spheroids from day 22 marked a change in behavior of the spheroids, and seeing that both AK and ATP content increased, it could be indicative of the initiation of apoptosis.[64–66] However, only viable cells would be able to form the daughter spheroids. Taking this into consideration, it was decided that although the NCI-H69V spheroid model was viable for 30 days, for the purposes of this study, the model would not be used beyond day 22. The formation of additional biomass (daughter spheroids) was uncontrollable and would affect reproducibility.

It was interesting that the AK per protein was significantly increased from day 22, at the same time that ATP per protein peaked for a second time, only to fall again on day 24. AK per protein continued to be significantly higher until day 30, with glucose consumption and ATP per protein also being significantly higher from day 28. Together with the loss of structural compactness, this suggested the presence of increased apoptosis at this stage of culture.

The ideal experimental window for the NCI-H69V spheroids was subsequently decided to be between days 14 and 22.

4.3 | Validation of the NCI-H69V spheroid model for anticancer screening

Two concentrations (IC_{25} and IC_{50}) of irinotecan were used to evaluate the effect of the treatment on the growth and viability of the NCI-H69V spheroids after daily treatment for 72 h. After 48 h exposure to both concentrations of irinotecan, the growth of the spheroids was significantly inhibited as indicated by the decrease in protein per

15206033, 2022, 4, Downloaded from https://aiche.onlinelibrary.wiley.com/doi/10.1002/btpr.3253 by Royal Danish Library, Wiley Online Library on [23/04/2026]. See the Terms and Conditions (https://onlinelibrary.wiley.com/terms-and-conditions) on Wiley Online Library for rules of use; OA articles are governed by the applicable Creative Commons License

spheroid, and the spheroids were also significantly smaller compared to the untreated control group. Irinotecan [IC_{50}] did not have a greater effect on protein and spheroid size than irinotecan [IC_{25}]. To evaluate the cytotoxic effects on the NCI-H69V spheroids, the intracellular ATP and extracellular AK levels were evaluated. The process of apoptosis requires adequate intracellular ATP levels and if ATP depletion occurs, the cells will still die, but under these circumstances, necrosis will occur.[65,66] Irinotecan [IC_{25}] decreased ATP per protein after just 24 h, but this was followed with a peak in ATP per protein, possibly due to the cells trying to recover. The simultaneous peak in AK release per protein after 48 h exposure, however, suggested that apoptosis of the cells took place as the ATP per protein markedly decreased after 72 h exposure. AK per protein decreased after 72 h exposure because there were fewer viable cells remaining to release AK, although it was still elevated relative to the untreated control. Irinotecan [IC_{50}] also caused a peak in AK per protein relative to the untreated control after 48 h exposure, but the effect on ATP per protein was much less severe after 72 h compared to irinotecan [IC_{25}]. After 72 h exposure, both concentrations of irinotecan reduced the glucose consumption of the spheroids to 0 mmol/L per μg protein.

Both concentrations of irinotecan that were used to treat the NCI-H69V spheroids caused a decrease in cell viability, protein content, and spheroid growth. The appearance of cell debris in the bioreactors were also evident after 48 h exposure, indicating possible cell death. The efficacy of irinotecan's cytotoxic activity on NCI-H69V spheroids have clearly been shown. It should be noted that the higher concentration of irinotecan was not significantly more detrimental to cell viability and growth than the lower concentration. Rossouw[55] administered 467 nM irinotecan (IC_{50}) daily to NCI-H69V 2D cells for 96 h, with the ATP per protein levels decreasing to half that of the untreated control only after 96 h exposure. In this study, the ATP per protein level decreased to half that of the untreated control in the NCI-H69V spheroids after only 72 h exposure.

Irinotecan [IC_{50}] has been previously found to accumulate in HCT 116 colon carcinoma spheroids, and were efficiently converted to its active metabolite (SN-38) by the viable cells after a 72 h treatment period.[23] This conversion of the pro-drug to the active metabolite is facilitated by the CE enzyme, which is found in high levels in SCLC tumors.[15] CE enzyme expression could be increased in the spheroids relative to the 2D cultures, resulting in a more effective conversion of irinotecan to its active metabolite within the spheroids. This would result in lower concentrations irinotecan being needed in the 3D model to obtain the same level of activity seen in 2D cultured cells.

5 | CONCLUSION

It can be concluded that the established functional NCI-H69V spheroid model is viable for at least 30 days, and can be used for experiments from 14 days of culture in the bioreactor. Some morphological characteristics of SCLC tumors was observed in the NCI-H69V spheroids following histological staining. The model is also highly reactive to the standard chemotherapeutic drug, irinotecan hydrochloride, and the results indicated that the model can be used for future screening of compounds for anticancer efficacy. The results also suggested that the conversion of irinotecan to its active metabolite (SN-38) was potentially more efficient in the spheroid model, again showing higher similarity to the in vivo tumors than their 2D counterparts. This could be a result of increase expression of the CE enzyme, as a significant correlation between CE activity and sensitivity to irinotecan treatment has previously been shown.[20] The NCI-H69V mini-tumor model can, therefore, serve as a new platform for the screening of new treatment compounds for SCLC.

ACKNOWLEDGMENTS

Krzysztof Wrzesinski and Chrisna Gouws would like to acknowledge the support of the COST action CA16119 (In vitro 3-D total cell guidance and fitness). This research was funded by the National Research Foundation (NRF) of South Africa (Grant number 116353 and 141964) and the South African Medical Research Council (MRC) (Self-Initiated Research Grant). Opinions expressed and conclusions arrived at, are those of the authors and are not necessarily to be attributed to the NRF or the MRC. The funders had no role in the design of the study, in the collection, analyses, or interpretation of data; in the writing of the manuscript, and in the decision to publish the results.

CONFLICT OF INTEREST

The authors declare no conflicts of interest. Krzysztof Wrzesinski is a director of CelVivo ApS.

AUTHOR CONTRIBUTION

The authors contributed to the following: the conception and design of the study – Hanna Svitina, Krzysztof Wrzesinski, and Chrisna Gouws; acquisition, analysis and interpretation of the data – Liezaan van der Merwe, Hanna Svitina, Clarissa Willers, Krzysztof Wrzesinski, and Chrisna Gouws; writing the article or revising it for important intellectual content – Liezaan van der Merwe, Hanna Svitina, Clarissa Willers, Krzysztof Wrzesinski, and Chrisna Gouws; supervision of the study – Hanna Svitina, Krzysztof Wrzesinski, and Chrisna Gouws. All the authors have read and approved the final published version of the manuscript.

DATA AVAILABILITY STATEMENT

Data is available on request.

ORCID

Chrisna Gouws https://orcid.org/0000-0001-5747-8214

REFERENCES

1. Huang Y, Hsu S. Acquisition of epithelial–mesenchymal transition and cancer stem-like phenotypes within chitosan-hyaluronan membrane-derived 3D tumour spheroids. *Biomaterials*. 2014;35:10070-10079.
2. Bray F, Ferlay J, Soerjomataram I, Siegel RL, Torre LA, Jemal A. Global cancer statistics 2018: GLOBOCAN estimates of incidence and mortality worldwide for 36 cancers in 185 countries. *CA Cancer J Clin*. 2018;68:394-424.

15206033, 2022, 4, Downloaded from https://aiche.onlinelibrary.wiley.com/doi/10.1002/btpr.3253 by Royal Danish Library, Wiley Online Library on [23/04/2026]. See the Terms and Conditions (https://onlinelibrary.wiley.com/terms-and-conditions) on Wiley Online Library for rules of use; OA articles are governed by the applicable Creative Commons License

3. Ferlay J, Soerjomataram I, Dikshit R, et al. Cancer incidence and mortality worldwide: sources, methods and major patterns in GLOBOCAN 2012. *Int J Cancer*. 2015;136:359-386.
4. Zhang W, Girard L, Zhang Y, et al. Small cell lung cancer tumours and preclinical models display heterogeneity of neuroendocrine phenotypes. *Transl Lung Cancer Res*. 2018;7:32-49.
5. Kamat CD, Shmueli RB, Connis N, Rudin CM, Green JJ, Hann CL. Poly (b-amino ester) nanoparticle delivery of TP53 has activity against small cell lung cancer in vitro and in vivo. *Mol Cancer Ther*. 2013;12: 405-415.
6. Pardo OE, Latigo J, Jeffery RE, et al. The fibroblast growth factor receptor inhibitor PD173074 blocks small cell lung cancer growth in vitro and in vivo. *Cancer Res*. 2009;69:8645-8651.
7. Vestergaard J, Pedersen MW, Pedersen N, et al. Hedgehog signalling in small-cell lung cancer: frequent in vivo but a rare event in vitro. *Lung Cancer*. 2006;52:281-290.
8. Zinn RL, Gardner EE, Dobromilskaya I, et al. Combination treatment with ABT-737 and chloroquine in preclinical models of small cell lung cancer. *Mol Cancer*. 2013;12:16.
9. Tardi PG, Dos Santos N, Harasym TO, et al. Drug ratio–dependent antitumour activity of irinotecan and cisplatin combinations in vitro and in vivo. *Mol Cancer Ther*. 2009;8:2266-2275.
10. Fushimi H, Kukui M, Morino H, et al. Detection of large cell component in small cell lung carcinoma by combined cytologic and histologic examinations and its clinical implication. *Cancer*. 1992;70:599-605.
11. Swarts DRA, Ramaekers FCS, Speel EM. Molecular and cellular biology of neuroendocrine lung tumours: evidence for separate biological entities. *Biochim Biophys Acta*. 2012;1826:255-271.
12. Helfrich BA, Kim J, Gao D, et al. Barasertib (AZD1152), a small molecule aurora B inhibitor, inhibits the growth of SCLC cell lines in vitro and in vivo. *Mol Cancer Ther*. 2016;15:2314-2322.
13. Oze I, Hotta K, Kiura K, et al. Twenty-seven years of phase III trials for patients with extensive disease small-cell lung cancer: disappointing results. *PLoS One*. 2009;4:e7835.
14. Wang S, Tang J, Sun T, et al. Survival changes in patients with small cell lung cancer and disparities between different sexes, socioeconomic statuses and ages. *Sci Rep*. 2017;7:1339.
15. Leonard SC, Lee H, Gaddy DF, et al. Extended topoisomerase 1 inhibition through liposomal irinotecan results in improved efficacy over topotecan and irinotecan in models of small-cell lung cancer. *Anticancer Drugs*. 2017;28:1086-1096.
16. Kondo R, Watanabe S, Shoji S, et al. A phase II study of irinotecan for patients with previously treated small-cell lung cancer. *Oncology*. 2018;94:223-232.
17. Horita N, Yamamoto M, Sato T, et al. Topotecan for relapsed small-cell lung cancer: systematic review and meta-analysis of 1347 patients. *Sci Rep*. 2015;5:15437.
18. Owonikoko TK, Zhang G, Deng X, et al. Poly (ADP) ribose polymerase enzyme inhibitor, veliparib, potentiates chemotherapy and radiation in vitro and in vivo in small cell lung cancer. *Cancer Med*. 2014;3: 1579-1594.
19. Warshamana-Greene GS, Litz J, Buchdunger E, García-Echeverría C, Hofmann F, Krystal GW. The insulin-like growth factor-I receptor kinase inhibitor, NVP-ADW742, sensitizes small cell lung cancer cell lines to the effects of chemotherapy. *Clin Cancer Res*. 2005;11:1563-1571.
20. Van Ark-Otte J, Kedde MA, Van Der Vijgh WJ, et al. Determinants of CPT-11 and SN-38 activities in human lung cancer cells. *Br J Cancer*. 1998;77:2171-2176.
21. Xu Y, Villalona-Calero MA. Irinotecan: mechanisms of tumour resistance and novel strategies for modulating its activity. *Ann Oncol*. 2002;13:1841-1851.
22. Johnson FM, Krug LM, Tran HT, et al. Phase I studies of imatinib mesylate combined with cisplatin and irinotecan in patients with small cell lung carcinoma. *Cancer*. 2006;106:366-374.
23. Liu X, Hummon AB. Quantitative determination of irinotecan and the metabolite SN-38 by nanoflow liquid chromatography-tandem mass spectrometry in different regions of multicellular tumour spheroids. *J Am Soc Mass Spectrom*. 2015;26:577-586.
24. Gardner EE, Lok BH, Schneeberger VE, et al. Chemosensitive relapse in small cell lung cancer proceeds through an EZH2-SLFN11 axis. *Cancer Cell*. 2017;31:286-299.
25. Früh M, De Ruysscher D, Popat S, Crinò L, Peters S, Felip E. Small-cell lung cancer (SCLC): ESMO clinical practice guidelines for diagnosis, treatment and follow-up. *Ann Oncol*. 2013;24:99-105.
26. Santo VE, Estrada MF, Rebelo SP, et al. Adaptable stirred-tank culture strategies for large scale production of multicellular spheroid-based tumour cell models. *J Biotechnol*. 2016;221:118-129.
27. Wang T, Wang L, Wang G, Zhuang Y. Leveraging and manufacturing in vitro multicellular spheroid-based tumour cell model as a preclinical tool for translating dysregulated tumour metabolism into clinical targets and biomarkers. *Bioresour Bioprocess*. 2020;7:35.
28. Pan E, Bogumil D, Cortessis V, Yu S, Nieva J. A systematic review of the efficacy of preclinical models of lung cancer drugs. *Front Oncol*. 2020;10:591.
29. Wong CH, Siah KW, Lo AW. Estimation of clinical trial success rates and related parameters. *Bios*. 2019;20:273-286.
30. Grimm D. U.S. EPA to eliminate all mammal testing by 2035, 2019 Available at: https://www.sciencemag.org/news/2019/09/us-epa-eliminate-all-mammal-testing-2035. Accessed October 30, 2020.
31. Fröhlich E. Issues with cancer spheroid models in therapeutic drug screening. *Curr Pharm Des*. 2020;26:1-12.
32. Kapałczyńska M, Kolenda T, Przybyła W, et al. 2D and 3D cell cultures–a comparison of different types of cancer cell cultures. *Arch Med Sci*. 2018;14:910-919.
33. Langhans SA. Three-dimensional in vitro cell culture models in drug discovery and drug repositioning. *Front Pharmacol*. 2018;9:1-14.
34. Hoarau-Véchot J, Rafii A, Touboul C, Pasquier J. Halfway between 2D and animal models: are 3D cultures the ideal tool to study cancer-microenvironment interactions? *Int J Mol Sci*. 2018;19:1-24.
35. Fennema E, Rivron N, Rouwkema J, Van Blitterswijk C, De Boer J. Spheroid culture as a tool for creating 3D complex tissues. *Trends Biotechnol*. 2013;31:108-115.
36. Krohn A, Ahrens T, Yalcin A, et al. Tumour cell heterogeneity in small cell lung cancer (SCLC): phenotypical and functional differences associated with epithelial-mesenchymal transition (EMT) and DNA methylation changes. *PLoS One*. 2014;9:e100249.
37. Khan MZ, Freshney RI, Murray AM, Merry S, Plumb JA, McNicol AM. Identification and characterisation in vitro of cells with a non-SCLC cell-like phenotype derived from a continuous SCLC cell line. *Anticancer Res*. 1991;11:1687-1695.
38. Kalluri R, Weinberg RA. The basics of epithelial-mesenchymal transition. *J Clin Invest*. 2009;119:1420-1428.
39. Van Staalduinen J, Baker D, Ten Dijke P, Van Dam H. Epithelial–mesenchymal-transition-inducing transcription factors: new targets for tackling chemoresistance in cancer? *Oncogene*. 2018;37:6195-6211.
40. Mehta G, Hsiao AY, Ingram M, Luker GD, Takayama S. Opportunities and challenges for use of tumour spheroids as models to test drug delivery and efficacy. *J Control Release*. 2012;164:192-204.
41. Edmondson R, Broglie JJ, Adcock AF, Yang L. Three-dimensional cell culture systems and their applications in drug discovery and cell-based biosensors. *Assay Drug Dev Technol*. 2014;12:207-218.
42. Santiago GT, Flores-Garza BG, Tavares-Negrete JA, et al. The tumour-on-Chip: recent advances in the development of microfluidic systems to recapitulate the physiology of solid tumours. *Materials*. 2019;12:2945-2984.
43. Fey SJ, Wrzesinski K. Bioreactor with lid for easy access to incubation cavity. EP2652120A4.
44. Calitz C, Hamman J, Viljoen A, Fey SJ, Wrzesinski K, Gouws C. Toxicity and anti-prolific properties of Xysmalobium undulatum water

15206033, 2022, 4, Downloaded from https://aiche.onlinelibrary.wiley.com/doi/10.1002/btpr.3253 by Royal Danish Library, Wiley Online Library on [23/04/2026]. See the Terms and Conditions (https://onlinelibrary.wiley.com/terms-and-conditions) on Wiley Online Library for rules of use; OA articles are governed by the applicable Creative Commons License

extract during short term exposure to two-dimensional and three-dimensional spheroid cell cultures. *Toxicol Mech Methods*. 2018;28:641-652.
45. Smit T, Calitz C, Willers C, et al. Characterisation of an alginate encapsulated LS180 spheroid model for anti-colorectal cancer compound screening. *ACS Med Chem Lett*. 2020;11:1014-1021.
46. Chaicharoenaudomrung N, Kunhorm P, Noisa P. Three-dimensional cell culture systems as an in vitro platform for cancer and stem cell modelling. *World J Stem Cells*. 2019;11:1065-1083.
47. Wrzesinski K, Fey SJ. After trypsinisation, 3D spheroids of C3A hepatocytes need 18 days to re-establish similar levels of key physiological functions to those seen in the liver. *Toxicol Res*. 2013;2:123-135.
48. Riss T, Moravec RA, Niles AL, et al. Cell viability assays. In: Markossian S, Sittampalam GS, Coussens NP, et al., eds. *Assay Guidance Manual*. Eli Lilly & Company and the National Centre for Advancing Translational Sciences; 2016:355-385.
49. Shandiz SS, Salehzadeh A, Ahmadzadeh M, Khalatbari K. Evaluation of cytotoxicity activity and NM23 gene expression in T47D breast cancer cell line treated with *Glycyrrhiza glabra* extract. *J Genet Resour*. 2017;3:47-53.
50. Fey SJ, Wrzesinski K. Determination of drug toxicity using 3D spheroids constructed from an immortal human hepatocyte cell line. *Toxicol Sci*. 2012;127:403-411.
51. Wrzesinski K, Frandsen HS, Calitz C, Gouws C, Korzeniowska B, Fey SJ. Clinostat 3D cell culture: protocols for the preparation and functional analysis of highly reproducible, large, uniform spheroids and organoids. In: Brevini TAL, Fazeli A, Turksen K, eds. *Next Generation Culture Platforms for Reliable in Vitro Models: Methods and Protocols*, *Methods in Molecular Biology*. Vol 2273. Humana Press; 2021:17-62.
52. D'Aniello C, Cermola F, Patriarca EJ, Minchiotti G. Vitamin C in stem cell biology: impact on extracellular matrix homeostasis and epigenetics. *Stem Cells Int*. 2017;2017:8936156.
53. Schneider CA, Rasband WS, Eliceiri KW. NIH image to ImageJ: 25 years of image analysis. *Nat Methods*. 2012;9:671-675.
54. Akçay A. The calculation of LD50 using probit analysis. *FASEB J*. 2013;27:1217-1218.
55. Rossouw MJ. Evaluation of the efficacy of selected anticancer compounds in multidrug resistant cell culture models. Msc Thesis. North-West University, Potchefstroom, South Africa; 2018.
56. Masuda N, Fukuoka M, Kusunoki Y, et al. CPT-11: a new derivative of camptothecin for the treatment of refractory or relapsed small-cell lung cancer. *J Clin Oncol*. 1992;10:1225-1229.
57. Schmittel A, Sebastian M, Fischer von Weikersthal L, et al. A German multicentre, randomized phase III trial comparing irinotecan-carboplatin with etoposide-carboplatin as first-line therapy for extensive-disease small-cell lung cancer. *Ann Oncol*. 2011;22:1798-1804.
58. National comprehensive cancer network (NCCN). Small cell lung cancer treatment regimens, 2020. Available at: https://www.cancertherapyadvisor.com/home/cancer-topics/lung-cancer/lung-cancer-treatment-regimens-landing-page/small-cell-lung-cancer-treatment-regimens/. Accessed November 9, 2020.
59. Nicholson SA, Beasley MB, Brambilla E, et al. Small cell lung carcinoma (SCLC): a clinicopathologic study of 100 cases with surgical specimens. *Am J Surg Pathol*. 2002;26:1184-1197.
60. Kijanska M, Kelm J. In vitro 3D spheroids and microtissues: ATP-based cell viability and toxicity assays. In: Markossian S, Sittampalam GS, Coussens NP, et al., eds. *Assay Guidance Manual*. Eli Lilly & Company and the National Centre for Advancing Translational Sciences; 2017:355-385.
61. Mosaad EO, Chambers KF, Futrega K, Clements JA, Doran MR. The microwell-mesh: a high-throughput 3D prostate cancer spheroid and drug-testing platform. *Sci Rep*. 2018;8:253.
62. Ahmann FR, Garewal HS, Schifman R, Celniker A, Rodney S. Intracellular adenosine triphosphate as a measure of human tumour cell viability and drug modulated growth. *In Vitro Cell Dev Biol*. 1987;23:474-480.
63. Klepinin A, Zhang S, Klepinina L, et al. Adenylate kinase and metabolic signalling in cancer cells. *Front Oncol*. 2020;10:660.
64. Jacobs AC, DiDone L, Jobson J, Sofia MK, Krysan D, Dunman PM. Adenylate kinase release as a high-throughput-screening-compatible reporter of bacterial lysis for identification of antibacterial agents. *Antimicrob Agents Chemother*. 2013;57:26-36.
65. Leist M, Single B, Naumann H, et al. Inhibition of mitochondrial ATP generation by nitric oxide switches apoptosis to necrosis. *Exp Cell Res*. 1999;249:396-403.
66. Eguchi Y, Shimizu S, Tsujimoto Y. Intracellular ATP levels determine cell death fate by apoptosis or necrosis. *Cancer Res*. 1997;57:1835-1840.

How to cite this article: van der Merwe L, Svitina H, Willers C, Wrzesinski K, Gouws C. A novel NCI-H69V small cell lung cancer functional mini-tumor model for future treatment screening applications. *Biotechnol. Prog*. 2022;38(4):e3253. doi:10.1002/btpr.3253

15206033, 2022, 4, Downloaded from https://aiche.onlinelibrary.wiley.com/doi/10.1002/btpr.3253 by Royal Danish Library, Wiley Online Library on [23/04/2026]. See the Terms and Conditions (https://onlinelibrary.wiley.com/terms-and-conditions) on Wiley Online Library for rules of use; OA articles are governed by the applicable Creative Commons License